Proceeding of the IEEE
International Conference on Robotics and Biomimetics
Dali, China, December 2019

Visual Servoing of Magnetic Swimming Robot Based on Mean Shift and Fast Template Matching Algorithm

Hongbiao Xiang[12*], Tilei Zhang[12], Mengwei Li[1], Shoujun Wang[12], Xiuping Yang[12]

1. Tianjin Key Laboratory for Advanced Mechatronic System Design and Intelligent Control, School of Mechanical Engineering
Tianjin University of Technology
Tianjin, 300384, China
xhb@tju.edu.cn

2.National Demonstration Center for Experimental Mechanical and Electrical Engineering Education
Tianjin University of Technology
Tianjin, 300384, China

***Abstract* - The actuation and control of mini-scale swimming robots have exhibit promising potential in limited and constrained environments, such as biomedical, micro-assembly and microfluidic applications. However, closed-loop control is still a challenging for the precision and repeatability in those applications. In this paper, a new type of soft-micro swimming robot based on magnetoelastic composite material is designed, and the swimmer can move freely on the water surface controlled by a rotating magnetic field with visual servoing. The visual feedback control strategy is proposed based on Mean Shift Algorithm and Fast Template Matching. The algorithm includes three parts: prediction, template matching, target positioning and template updating. To understand the characteristics of the swimmer, the relationship between swimming speed and magnetic field strength and frequency is verified by the algorithm in experiments. Furthermore, the proposed path following method with visual servoing applied in this control system. The experimental results show that the algorithm runs fast, has high accuracy and good real-time performance, and can provide great potential in mini-scale robot applications.**

Index Terms* - *Swimming robot, Magnetoelastic composite material, Template matching, Mean Shift

I. INTRODUCTION

Cable-less mobile microrobots have shown great potential for various application, such as micro assembly, biomedical operation, vitro tasks and so on. Because they can work in small or narrow space where the conventional actuators or robots cannot access. In recent years, micro swimming robots have received extensive attention from researchers [1-3]. Due to the mini-scale and hard to realize the on-board energy, magnetic fields control method has become a great choice [4-6].

However, the stability and accuracy control of micro swimming robots are still a challenge for researchers in those applications, especially requiring more optimal strategies in complex task. The micro swimmer can take some simple task in present, and most of them are controlled by open-loop method. Due to the turbulence in low Reynolds numbers, random disturbance, modelling error, and other unexpected factors, the close-loop control strategy for micro swimmer become necessary and important, and Optimized tracking algorithm is required for the visual feedback of swimming robot. Furthermore, Visual servoing has shown great capacity in large-scale robots and tracking for target tracking in the past decades, and only in recent years it has applied in micro robot.

Target tracking technology has flourished and developed in recent years [7-9]. It is an important technology in those application of man-machine interaction, monitoring, intelligent transportation system and so on [10-12]. Mean Shift Algorithm is a classic and widely used algorithm applied in various fields. However, researchers are constantly updating and improving this algorithm. Y Chong extended and analyzed the Mean Shift, which is a simple iterative procedure to shifts each data point to the average of data points in its neighborhood [13]. Aiming at the rapid movement and drift problem of object tracking algorithm, Z Wang proposed a new object tracking algorithm combining YOLO with Mean shift [14]. On the count of the ground similarities and scale change and target occlusion in the process of target tracking, a scale and orientation adaptive mean shift tracking with corrected background-weighted histogram is proposed to solve this problem [15-16]. Yilmaz presents an object tracking method based on the asymmetric kernel mean shift, in which the scale and orientation of the kernel adaptively change depending on the observations at each iteration [17-18]. In recent years, the closed-loop control method has come into application for micro swimmers. T Xu presents a closed-loop control method base on Image-Based Visual Servoing (IBVS), applied on helical micro swimmers for 3D arbitrary path following at low Reynolds numbers [19]. Oulmas proposed a 3D closed-loop path following algorithm based on Position-Based Visual Servoing (PBVS) [20]. The Meanshift algorithm can achieve the high speed for identification, but it is easy to be affected by background change. Meanwhile the template matching algorithm needs a lot of calculation, which is not conducive to the real-time performance of the experiment system. Therefore, this paper proposes a swimming robot motion recognition and tracking algorithm, which is compatible with the advantage of mean shift and fast template matching. Then the visual servoing based on this algorithm is carried out in motion control strategy. This visual servoing strategy can execute complex tasks and suppress interference in low Reynolds numbers, which also can apply in targeted drug delivery, transporting individual cells and so on.

In the following article, Section II introduce the structural and discussed the mathematical modeling of the swimming robot, and analyze the swimming characteristics with the periodic control signals of 3D Helmholtz coils. The principle of the recognition and tracking algorithm is proposed in Section III. Then, the path following error presents and shows the accuracy of the tracking path in experiments based on the visual

978-1-7281-6321-5/19//$31.00 ©2019 IEEE

servoing control strategy. Finally, Section V concludes the paper.

II. Modeling

A. Control system setup

As shown in Fig. 1, the experiment system is composed of Industrial Personal Computer, LabVIEW CompactDAQ module, power amplifier(HEA-1050), high speed camera(Mako U-130B) and 3D Helmholtz coils(3HLY5-130), micro swimming robot (YMM-E-15-7,NdFeB and Ecoflex 00-01). The LabVIEW module can output three channel signals to control 3D Helmholtz coils, which can generate arbitrary direction uniform magnetic field in XYZ coordinate space. The cameras are used to collect the motion information of micro swimming robot on water surface, including position and angle on top view, and motion and morphology on side view. As previous studies, the swimming robot consists of two magnetic blocks and flexible joint. The two magnetic blocks are composed of magnetoelastic composite material with same size but opposite magnetization direction, meanwhile the joint part, using silicone rubber, is responsible for linking the two magnetic blocks and bending up and down through magnetic moment.

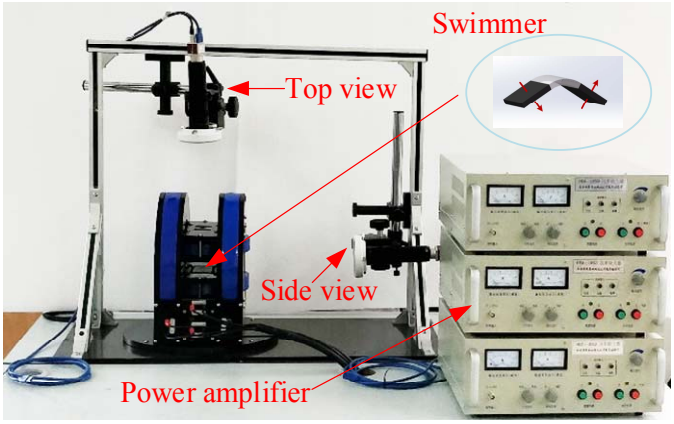

Fig. 1 Control system setup

B. Modelling and force analysis

The motion and morphology of a swimming robot depend on its material properties, geometry and external magnetic field. Considering the magnetic blocks are rigid and cannot deform, the deformation of swimmer mainly lies on the flexible joint part. The force analysis is shown in Fig. 2

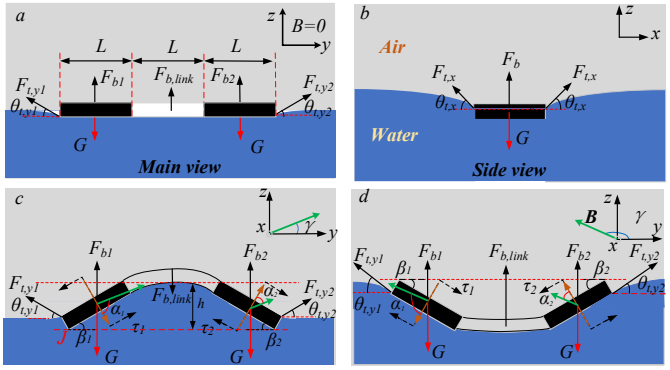

Fig. 2 Force analysis of swimming robot. The swimming robot structural is described in (a). The swimmer deforms when a external magnetic field is applied and interacts with the water surface. The swimmer with the forces and torques are qualitatively drawn in the main view, side view in (b–d), respectively.

The swimmer is subjected to the gravity, magnetic moment, buoyancy and surface tension of the water. To simplify the model, we ignore the mass of joint because of its smaller density. The surface tension is F_t, and the direction is along the tangent of the water surface at the contact point of the robot. The angle between tension and horizontal plane is θ_t. The tension on the width edge of the soft robot is expressed by $F_{t,y}$, and the angle between them and the horizontal plane is $\theta_{t,y}$. To simplify the model, we only consider the effect of tension in the width direction of the swimmer. $F_{t,res}$ is the resultant force of tension in the vertical direction. F_b is the buoyancy of the robot. F_{b1} and F_{b2} represent the buoyancy force on the head and tail of the robot respectively. $F_{b,link}$ is the buoyancy of the joint.

$$\begin{cases} F_{t,res} + F_{b,res} = 2G \\ F_{t,res} = F_{t,y1}\sin\theta_{t,y1} + F_{t,y2}\sin\theta_{t,y2} \\ F_{b,res} = F_{b1} + F_{b2} + F_{b,link} \end{cases} \tag{1}$$

The torque balance equation is deduce based on J point as the reference point.

$$M_G + M_t + M_b + \tau_1 - \tau_2 = 0 \tag{2}$$

M_G is the torque from gravity at point J

$$M_G = -\frac{3}{2}LG\cos\beta_1 - \left(w_{yL} + \frac{1}{2}L\cos\beta_2\right)G \tag{3}$$

M_t is the torque from surface tension at point J

$$M_t = \left(L\cos\beta_1 + w_{yL} + \frac{1}{2}L\cos\beta_2\right)F_{t,y2}\sin\theta_{t,y2} \tag{4}$$

M_b is the torque from buoyancy at point J

$$\begin{aligned} M_b = {} & \frac{L}{2}F_{b1}\cos\beta_1 + F_{b,link}\left(L\cos\beta_1 + \frac{w_{yL}}{2}\right) \\ & + F_{b2}\left(L\cos\beta_1 + w_{yL} + \frac{1}{2}L\cos\beta_2\right) \end{aligned} \tag{5}$$

where w_{yL} is the distance of the joint in the x direction. τ_1 and τ_2 represent the magnetic moment of the two blocks

$$\begin{cases} \tau_1 = MBV\sin\alpha_1 \\ \tau_2 = MBV\sin\alpha_2 \end{cases} \tag{6}$$

where M, B and V are the magnetization, magnetic flux density and the volume of the block respectively. α_1 and α_2 represent

the angle between the magnetization direction of magnetic blocks and the direction of magnetic flux density B respectively.

Referring to the swimming model of Geoffrey Taylor, the swimming speed of the robot is

$$v = \frac{2\pi^2}{3L}(AR)^2 f = \frac{2\pi^2}{3L}\left(\frac{hR}{2}\right)^2 f \tag{7}$$

where R is related to the natural frequency f_n of the miniature swimming robot. When the magnetic field frequency is less than f_n, R is 1; when the magnetic field frequency is greater than or equal to f_n, R is $(f_n/f)^2$. According to the experimental results, we get the natural frequency of the swimmer is 32.5Hz.

C. Control of The Swimming Robot

When the swimmer is supposed to swim along a certain direction on the *xy* plane, the rotation magnetic field should be setup on this plane and parallel to the z-axis. As shown in Fig. 3, the swimmer moves along the direction on *xy* plane, and the angle with *x*-axis is φ. Meanwhile the rotating magnetic field was generated along the angle γ counter-clockwise. The steering control of the robot in the magnetic field can realize through changing the φ angle.

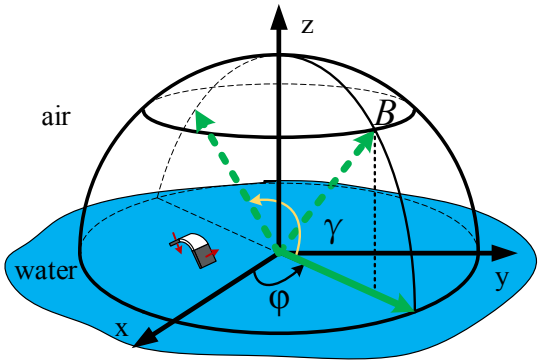

Figure. 3 Magnetic field at spherical coordinates system

As shown in Fig. 4, setting the certain magnetic flux density (B = 80Gs) and the frequency (f=10Hz), 6 different posture of swimming morphology in one period is presented by side view camera. The robot continuously deforms along the water surface under the control of the waveform, causing the robot to move linearly on the water surface.

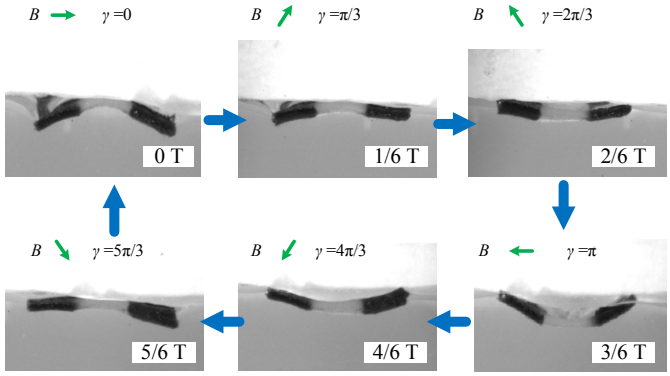

Figure. 4 6 different posture of swimming morphology in one period

Ⅲ. Mean Shift and Fast Template Matching Algorithm

A. Principle

The traditional mean shift algorithm is liable to be affected by the tracking target image pixels and the background image pixels. When the background area included in the target model area has more pixels or the background is constantly changing, the target is easy to lost. The traditional template matching algorithm is a simple tracking algorithm, but it is computationally intensive and is not suitable for high real-time requirements. In this paper, the target position is predicted by using the mean shift method, then template matching is used in a small range of the predicted position area, which improves the efficiency of template matching. The algorithm is based on mean shift and fast template matching algorithm (MSFTM). The specific implementation steps are as follows.

It is assumed that the center coordinate of the target area obtained by the *k-1* frame image is X_{k-1}, and the updated target template is T_k. If the target area of the *k*th frame has n pixels, that is, $\{X_i, i=1,2,\cdots,n\}$, the probability density of the target model feature $Q_u(u=1,2,\cdots,m)$ is

$$Q_u = C\sum_{i=1} k\left(\left\|\frac{X_{k-1}-X_i}{h}\right\|^2\right)\delta\left[b(X_i)-u\right] \tag{8}$$

Where m is the numbers of elements in the feature space. C is the normalization coefficient of the target model. $k(x)$ is the kernel function for pixel weighting; h is the bandwidth. $\delta[b(Xi)-u]$ is the Kronecker delta function, used to determine whether the pixel value X_i is equal to the uth feature value in the target region.

In the same way, if the central coordinate of the candidate target region is Y, then the probability distribution of the candidate target model is:

$$P_u(Y) = C_1\sum_{i=1} k\left(\left\|\frac{Y-X_i}{h}\right\|^2\right)\delta\left[b(X_i)-u\right] \tag{9}$$

C_1 is the normalization coefficient of the candidate target model.

When using mean shift algorithm to predict the position of moving target, similarity function is required to measure the matching degree between target model and candidate model. In other words, it is the similarity between $P_u(Y)$ and Q_u. In this paper, Bhattacharyya coefficient is selected as the similarity function

$$P'(Y) = \sum_{u=1}^{m}\sqrt{P_u(Y)Q_u} \tag{10}$$

The matching degree of candidate target and template target increases with the value of $P'(Y)$. The center coordinate of the target region obtained by the *(k-1)*th frame image is X_{k-1}, and the center coordinate of the iterative target region of the *k*th frame obtained by the Bhattacharyya coefficient is

$$X_k = \frac{\sum_{i=1} g\left(\left\|\frac{Y-X_i}{h}\right\|^2\right) w_i X_i}{\sum_{i=1} g\left(\left\|\frac{Y-X_i}{h}\right\|^2\right) w_i} \tag{11}$$

where

$$g(x) = -k(x), w_i = \sum_{i=1}^{m} \sqrt{\frac{Q_u}{P_u(Y)}} \delta\left[b(X_i) - u\right]$$

Then a search window *S(k)* is generated, based on the prediction position X_k obtained by the mean shift algorithm. The template matching is performed to obtain a possible position X_p, and to obtain a best matching degree *N* between the target template T_k and the search window *S(k)*. If the matching degree N is greater than the threshold ε, the matching result can be used as the tracking result of the *k*th frame image, otherwise the target position predicted by the mean shift algorithm will become the tracking result of the *k*th frame image.

The algorithm flow chart is shown in Fig. 5.

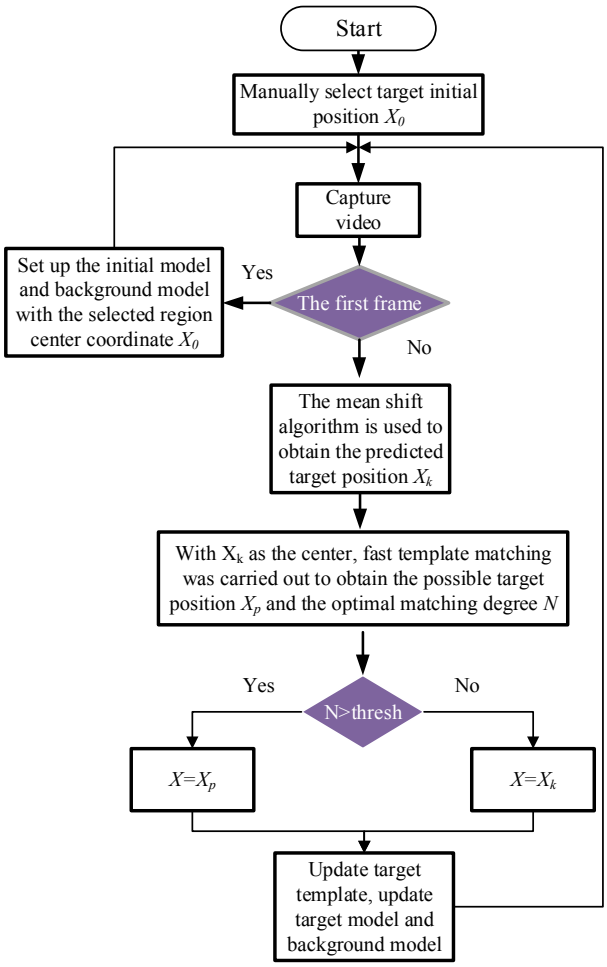

Figure. 5 MSFTM algorithm flow chart

B. *Tracking Experiment*

The tracking experiments of the swimmer on the *xy* plane is collected by top view camera. As shown in Fig. 6, the tracking effect of MSFTM algorithm is compared with the traditional mean shift algorithm.

As the tracking time increases, the accuracy of the mean shift decreases or the tracking target is easy to lost, and the MSFTM algorithm can accurately track the target. When the background become complex, the MSFTM algorithm is more robust and the accuracy of trajectory track is improved. The MSFTM algorithm has high accuracy and good stability. It not only can track target deformation and local occlusion, but also can track the complex background, especially when the illumination changes greatly. It also shown good real-time performance and accurately tracking for moving objects.

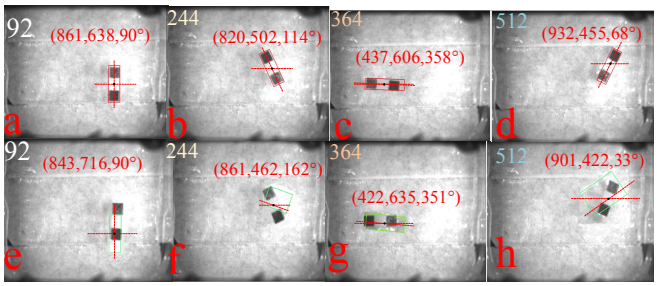

Fig. 6 (a-d) The MSFTM algorithm tracks the results, (e-h) is the result of mean shift algorithm.

As shown as Table I, the results are obtained by tracking 1000 frames pictures with two algorithms above. MSFTM is a swimming robot motion recognition and tracking algorithm based on mean shift and fast template matching, which can effectively improve the recognition accuracy without affecting the identification cycle.

TABLE I
COMPARISON OF TWO TRACKING ALGORITHMS

	Comparison of tracking effect		
	Category	Mean Shift	MSFTM
1	Accuracy rate (%)	61.5	82.3
2	Identification time(ms)	18.11	20.04

IV. EXPERIMENTAL RESULTS

A. *Control Strategy*

According to the equation (7), the swimmer's speed is related to its deflection's amplitude square and frequency (under 32.5Hz), which can be controlled by the amplitude, frequency, and direction of magnetic flux density B in XYZ space. As shown in Fig. 7, a visual servoing method is set up based on the information of the swimmer's present position and direction from visual feedback, the position and the direction are controlled in real-time, using a proportional (PID) controller and a proportional-integral (PI) controller, respectively. The desire path is *P*, which include the information displacement x_d in *x*-axis direction, displacement y_d in *y*-axis direction, and the swimmer steer angle θ_d. The present position (x_c, y_c) and present angle θ_c are get from the image processing through MSFTM.

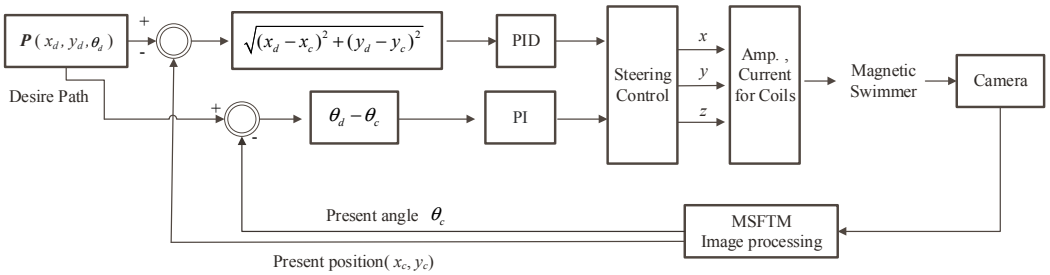

Fig. 7 Block diagram of the visual servoing system based MSFTM for the swimmer.

B. *Steering and straight lines Results*

The swimming robot moves on the water surface, controlled by rotating magnetic field. The speed and the steer angle of the swimmer are related to parameters of the control signals.

When the steering motion of the swimmer is executed, the steer error between the desire angle and present angle base on MSFTM algorithm is shown in Fig. 8.

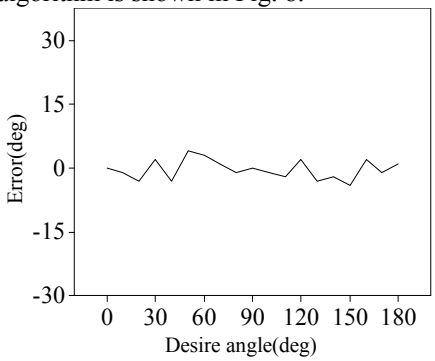

Fig. 8 Steer error of steering motion.

When the swimmer moves in straight line, the speed is related to the magnetic strength and frequency with rotating magnetic field. As shown in Fig. 9, The solid line data comes from the experimental results, the dashed data comes from the analysis results of the modeling process in Section II. When the magnetic field frequency is constant (11Hz), the displacement is linear with time, and the slope of displacement is increased with the magnetic strength. When the magnetic field strength is constant (70Gs), the displacement is linear with time, and the slope of displacement is increased with the magnetic frequency.

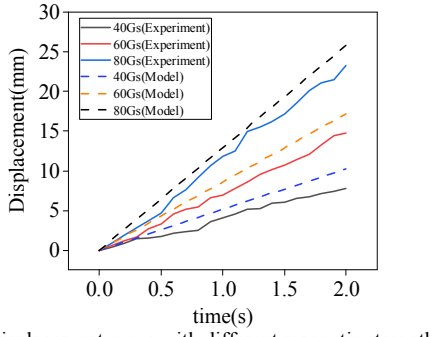

(a)Displacement curve with different magnetic strength

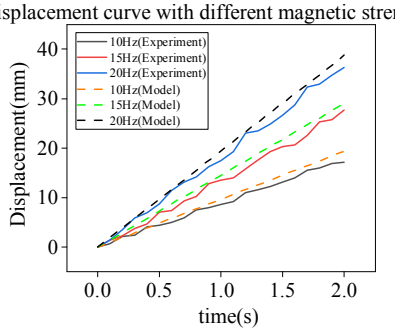

(b)Displacement curve with different frequencies

Fig. 9 Displacement curve with magnetic strength and frequencies.

C. *Path Following Results*

The path following experiments are carried out at constant frequency (f=11Hz) and strength (B=60Gs). The path “O” and “N” are performed using visual serviong method based on MSFTM algorithm.

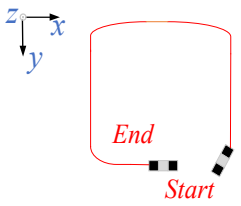

(a) Path "O"

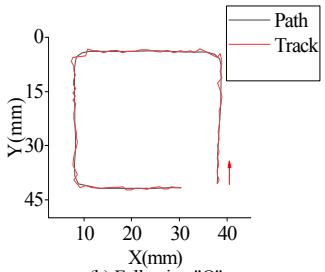

(b) Following "O"

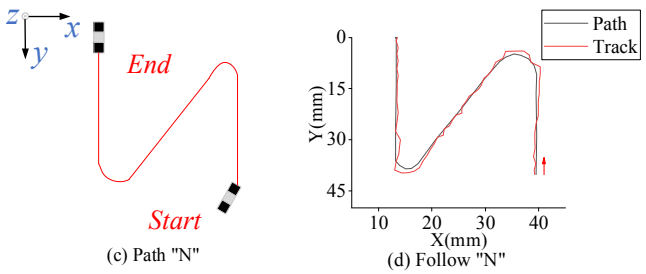

(c) Path "N" (d) Follow "N"

Figure. 10 (a) (c) are Desire path, (b) (d) are tracking curves.

The displacement errors and steering errors are recorded in Fig. 11. Angle error is less than ±5 degree, the displacement error is less than 3mm, and the large fluctuations of displacement error are happened in the fast turning corner. The displacement error was calculated by the root-mean square deviation (RMSD). According to the experimental results, the visual servoing control strategy based on MSFTM algorithm can achieve stable and accurate tracking of the swimmer.

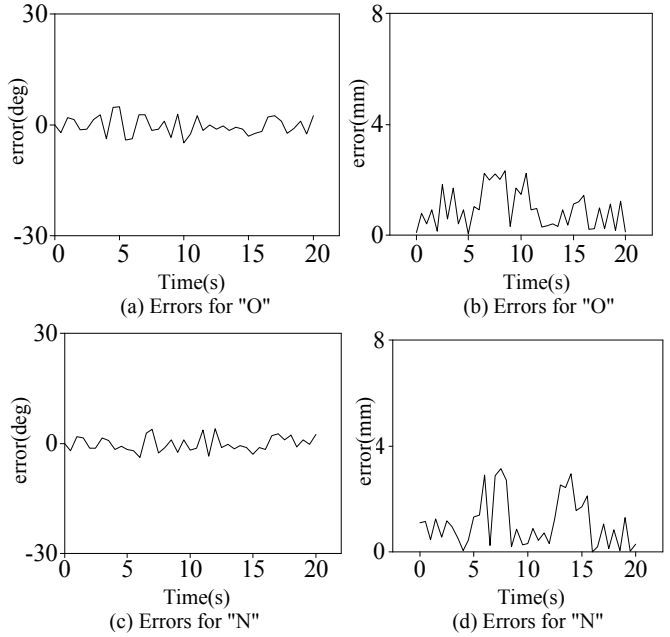

(a) Errors for "O" (b) Errors for "O"

(c) Errors for "N" (d) Errors for "N"

Figure. 11 Steering and displacement errors of path "O" and "N" in (a)-(d).

V. Conclusion

In this paper, we proposed an algorithm for motion recognition and tracking of swimming robots, based on mean shift and fast template matching algorithm. Then the visual servoing based on this algorithm is implemented in motion control strategy. The experimental results show that the swimmer can swim accurately and stably along different desire path. The MSFTM algorithm has high accuracy and good real-time performance in tracking the target, and can effectively feedback the position and steer angle of the tracking target. In future works, we will use method to 3D arbitrary tracking path for swimming under water.

Acknowledgment

The author would like to thank Tianjin University of technology and Tianjin University, and this work was supported by National key research and development Program of China under Grant 2017YFB1302100 and Tianjin Natural Science Foundation (NO. 18JCYBJC19300).

References

[1] K. E. Peyer, "Bacteria-Inspired Magnetic Polymer Composite Microrobots," *Proceedings of the Second international conference on Biomimetic and Biohybrid Systems*. Springer, Berlin, Heidelberg, 2013.

[2] M. Suter, et al, "Superparamagnetic microrobots: fabrication by two-photon polymerization and biocompatibility," *Biomedical Microdevices*, vol.15, no. 6, pp.997-1003, 2013.

[3] C. Peters, O. Ergeneman, B. J. Nelson, C. Hierold, "Superparamagnetic swimming microrobots with adjusted magnetic anisotropy," *Micro Electro Mechanical Systems (MEMS), 2013 IEEE 26th International Conference on IEEE*, 2013.

[4] H. Xiang, M. Trkov, K. Yu, and J. Yi, "A stick-slip interactions model of soft-solid frictional contacts," *Journal of Dynamic Systems, Measurement, and Control,* vol. 141, no. 4, 2019.

[5] J. Zhang, and E. Diller, "Untethered Miniature Soft Robots: Modeling and Design of a Millimeter-Scale Swimming Magnetic Sheet," *Soft Robotics*, 2018.

[6] H. Xiang, M. Trkov, K. Yu, and J. Yi, "A stick-slip interactions model of soft-solid frictional contacts," *Journal of Dynamic Systems, Measurement, and Control,* vol. 141, no. 4, 2019.

[7] Ivorra. E, et al, "Intelligent Multimodal Framework for Human Assistive Robotics Based on Computer Vision Algorithms," *Sensors (Basel)*, vol. 18, no. 8, Jul 2018.

[8] H.-B. Liu, et al, "Algorithm for real-time image processing in the robot soccer," *Trans Tech Publications*, vol. 143-144, pp. 737-7418, 2012.

[9] Caelli. T and S. Nagendran, "Fast edge-only matching techniques for robot pattern recognition," *Computer vision, graphics, and image processing*, vol. 39, no, 2. pp. 131-143, 1987.

[10] C.-Y. Zhang, X.-M. Zhang, "The Technology Challenge and Application Idea of Human-Computer Interaction Driven by Artificial Intelligence," *Digital* Technology *& Application,* vol. 36, no. 05, pp. 206-207, 2018.

[11] G.-R. Liu, et al, "The research and design of embedded wireless video monitoring system," *IEEE Computer Society*, pp. 2795-2794, 2011.

[12] W.-H. Ruan, Z.-H. Li, Z. Huang, "Research on detection and tracking of moving objects in intelligent transportation system based on laser scanning," Laser Journal, vol. 40, no. 4, pp. 50-54, 2019.

[13] Y.-Z. Chong, "Mean shift, mode seeking, and clustering," *IEEE Transactions* on *Pattern Analysis and Machine Intelligence,* vol. 17, no. 8, pp. 790-799, 1995.

[14] Z.-M. Wang, N. Duan, and L. Fan, "Object tracking algorithm fused with YOLO detection and Meanshift," *Computer Engineering and Applications*, vol. 55, no.10, pp. 186-192+212, 2019.

[15] H. Zheng, et al, "Scale and orientation adaptive mean shift tracking with corrected background-weighted histogram," *Computer Engineering and Applications*, vol. 52, no. 22, pp. 192-197, 2016.

[16] Comaniciu. D, et al, "Real-time tracking of non-rigid objects using mean shift," IEEE *Conference on Computer Vision and Pattern Recognition*, vol. 2, pp. 142-149, 2000.

[17] Comaniciu. D, P. Meer, "Mean shift: A robust approach toward feature space analysis," *IEEE Transactions on Pattern Analysis and Machine Intelligence*, vol. 24, no. 5, pp. 603-619, 2002.

[18] Yilmaz. A, "Kernel-based object tracking using asymmetric kernels with adaptive scale and orientation selection," *Machine Vision and Applications*, vol. 22, no. 2, pp.255-268, 2011.

[19] T.-T. Xu, et al, "Visual Servoing of Miniature Magnetic Film Swimming Robots for 3-D Arbitrary Path Following," *IEEE Robotics and Automation Letters*, vol. 4, no. 4, pp. 4185-4191, 2019.

[20] A. Oulmas, N. Andreff, and S. Regnier, "Closed-loop 3d path following of scaled-up helical microswimmers," *In IEEE International Conference on Robotics and Automation*, pp. 1725–1730, 2016.